ACADEMIC
PRESS

Electron spin–lattice relaxation in radicals containing two methyl groups, generated by γ-irradiation of polycrystalline solids

James R. Harbridge, Sandra S. Eaton, and Gareth R. Eaton*

Department of Chemistry and Biochemistry, University of Denver, Denver, CO 80208-2436, USA

Received 21 June 2002; revised 3 September 2002

Abstract

The effects of methyl rotation on electron spin–lattice relaxation times were examined by pulsed electron paramagnetic resonance for the major radicals in γ-irradiated polycrystalline α-amino isobutyric acid, dimethyl-malonic acid, and L-valine. The dominant radical is the same in irradiated dimethyl-malonic acid and α-amino isobutyric acid. Continuous wave saturation recovery was measured between 10 and 295 K at S-band and X-band. Inversion recovery, echo-detected saturation recovery, and pulsed electron–electron double resonance (ELDOR) data were obtained between 77 and 295 K. For the radicals in the three solids, recovery time constants measured by the various techniques were not the same, because spectral diffusion processes contribute differently for each measurement. Hyperfine splitting due to the protons of two methyl groups is resolved in the EPR spectra for each of the samples. Pulsed ELDOR data were obtained to characterize the spectral diffusion processes that transfer magnetization between hyperfine lines. Time constants were obtained for electron spin–lattice relaxation (T_{1e}), nuclear spin relaxation (T_{1n}), cross-relaxation (T_{x1}), and spin diffusion (T_s). Between 77 and 295 K rapid cross-relaxation ($\Delta M_s = \pm 1$, $\Delta M_I = \mp 1$) was observed for each sample, which is attributed to methyl rotation at a rate that is approximately equal to the electron Larmor frequency. The large temperature range over which cross-relaxation was observed suggests that methyl groups in the radical and in the lattice, with different activation energies for rotation, contribute to the rapid cross-relaxation. Activation energies for methyl and amino group rotation between 160 and 1900 K (1.3–16 kJ/mol) were obtained by analysis of the temperature dependence of $1/T_{1e}$ at S-band and X-band in the temperature intervals where the dynamic process dominates T_{1e}.
© 2002 Elsevier Science (USA). All rights reserved.

1. Introduction

Electron spin–lattice relaxation times reflect the environment of the paramagnetic species and can be used to obtain a wide variety of information, including insights into electronic structure, dynamic processes, and distances between centers with differing relaxation times [1]. To obtain reliable values of spin–lattice relaxation times (T_{1e}) it is necessary to understand how other processes may contribute to experimental recovery curves obtained by various techniques and to distinguish these processes from spin–lattice relaxation. In this study we compare inversion recovery, echo-detected saturation recovery (ED-SR), long-pulse continuous wave saturation recovery (CW-SR), and electron–electron double resonance (ELDOR) methods of measuring T_{1e} for radicals with resolved couplings to the protons of two methyl groups. By comparing the temperature dependence of spin–lattice relaxation times for these three samples, measured by different methods, we seek a clearer understanding of the effects of methyl rotation on electron spin relaxation and on spectral diffusion processes.

Relaxation requires transfer of energy from the electron spin system to the lattice (the surroundings), which can occur via a variety of processes. In the direct process there is a match of the Zeeman energy with a phonon energy, so that there can be a direct transfer of energy from the spin system to the lattice phonon bath. The direct process often dominates spin–lattice relaxation at temperatures below 10 K [1–8]. The Raman process is a two-photon process in which the Zeeman energy is equal to the difference between the energies absorbed and emitted for a virtual excited state with an energy that is less than the Debye temperature [1–4,9].

---

* Corresponding author. Fax: 1-303-871-2254.
   E-mail address: geaton@du.edu (G.R. Eaton).

The Raman process has been found to dominate spin–lattice relaxation for some $S = 1/2$ systems in glassy matrices or magnetically dilute solids between 10 and 200 K [1,10]. Thermally activated dynamic processes, which include methyl group rotation, amino group rotation, or movement of a hydrogen-bonded proton, can absorb energy from the spin system when the frequency of the process is comparable to the electron Larmor frequency [11–18]. Other processes that may contribute to electron spin relaxation are Orbach–Aminov processes [1–4,19] and local vibrational modes [19–21]. The mechanisms by which these processes affect spin–lattice relaxation include modulation of hyperfine interaction [22], of spin–orbit coupling [23,24], or of zero-field splitting [25]. If a single process dominates the relaxation at a particular temperature, the experimental recovery curve is a single exponential.

The effects of methyl and amino group rotation on nuclear spin relaxation have been extensively studied by NMR [11–16], but the effects on electron spin relaxation have been much less thoroughly examined [10,26–28]. Obtaining a true value for T_1 by pulsed NMR is much easier than by pulsed EPR because the NMR spectral width typically is narrower than the excitation bandwidth of the pulses used to obtain the recovery curves, so most spectral diffusion processes are eliminated. However, the EPR spectral width often is greater than the excitation bandwidth of the pulses, so spectral diffusion processes can contribute to the recovery curves if these processes transfer spin magnetization out of the observation bandwidth. The observation bandwidth depends on the experiment performed. If the time constant for a spectral diffusion process is shorter than T_{1e}, but long enough to be observable, the apparent time constant for return to equilibrium will be shorter than T_{1e}. Several spectral diffusion processes in solids have been described in the literature [1,29–42]. Nuclear spin relaxation ($\Delta M_s = 0$, $\Delta M_I = \pm 1$) is a spectral diffusion process that transfers spin polarization from one nuclear spin state to another. Cross-relaxation transfers spin polarization between Zeeman frequencies by processes that involve the mutual flip of two unlike spins. In the present application it is restricted to the case in which $\Delta M_s = \pm 1$, $\Delta M_I = \mp 1$. The time constants for cross-relaxation and nuclear relaxation between resolved hyperfine lines can be measured using pulsed electron–electron double resonance (ELDOR). Spin diffusion is a spectral diffusion process that moves magnetization within an inhomogeneously broadened line. In some cases the contribution of spectral diffusion processes to the observed recovery curve can be decreased if the pump time that is used to excite a spin transition is much longer than T_{1e}.

In this study, the effects of methyl rotation on spin–lattice relaxation and spectral diffusion processes are examined for radicals with hyperfine couplings to the
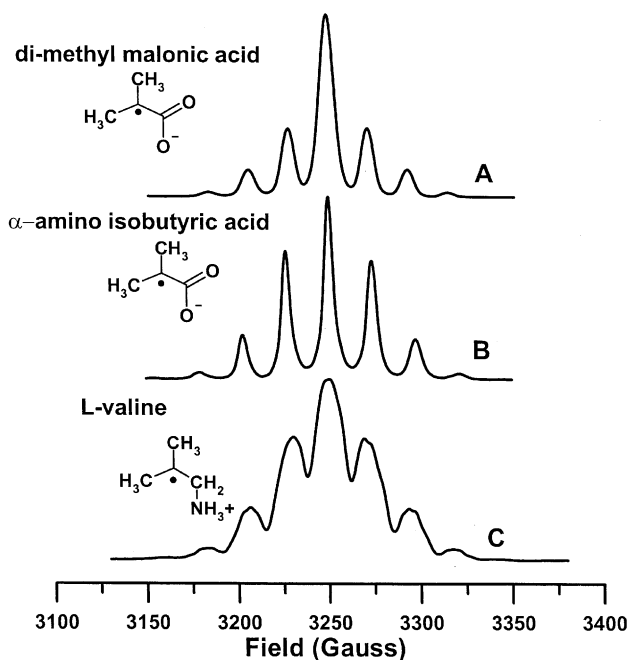

Fig. 1. Room temperature EPR-CW absorption spectra of the radicals in the three polycrystalline irradiated samples studied. First derivative spectra were obtained at X-band with 0.5 G modulation amplitude and 100 kHz modulation frequency and computer integrated. (A) dimethyl-malonic acid radical, (B) α-amino isobutyric acid radical, (C) L-valine radical.

protons of two methyl groups. γ-Irradiation of dimethyl-malonic acid and of α-amino isobutyric acid produces the same radical. Equivalent coupling to six methyl protons is resolved in the EPR spectrum of this radical at room temperature ($A_H \sim 22$ G) (Figs. 1A and B). In the EPR spectrum of the radical in γ-irradiated L-valine at room temperature there is resolved coupling to the protons of two methyl groups ($A_H \sim 20$ G) and to a CH_2 group ($A_H \sim 20$ G), and partially resolved coupling to a nitrogen ($A_N \sim 5.5$ G) (Fig. 1C).

2. Experimental

2.1. Samples

Polycrystalline samples of α-amino isobutyric acid, (99%, Aldrich, Milwaukee, WI), dimethyl-malonic acid, (99%, Aldrich), and L-valine (99$^+$%, Aldrich) were irradiated at room temperature with a ^{60}Co source to a dose of approximately 6 Mrad (60 kGy). After irradiation the samples were stored in air at room temperature. Experiments were performed weeks to years after irradiation. Spin concentrations were determined by comparison of double-integrated first-derivative CW spectra with spectra for a 0.53 mM solution of 2,2,6,6-tetra-methyl-piperidinyl-1-oxy (Aldrich Chemical, Milwaukee, WI) in toluene. For irradiated L-valine and

α-amino-isobutyric acid the spin concentrations were 4×10^{18} and 3.5×10^{18} spins/cm^3, respectively, with little time dependence detected. For irradiated dimethylmalonic acid the spin concentration gradually decreased from about 7×10^{17} to 3×10^{17} spins/cm^3, over the several year time-span during which experiments were performed.

2.2. Spectroscopy

X-band (ca. 9.1 GHz) CW-SR measurements were made using a locally constructed spectrometer [43]. Temperatures between 10 and 70 K were obtained using an Oxford ESR900 flow cryostat. Temperature at the sample, as a function of liquid helium flow and heater setting, was calibrated by replacing the sample with a tube containing a thermocouple immersed in 1:1 water:glycerol. The temperature at the sample was strongly dependent upon the helium flow rate, which causes as much as 2 K uncertainty in the temperature. Temperatures between 77 and 230 K were obtained using a Varian liquid nitrogen cooled gas flow system. Temperatures above 230 K were obtained by flowing N_2 gas through a coil submersed in a dry ice–acetone bath. Between 77 and 300 K the temperature was measured with a thermocouple positioned near the top of the sample and the uncertainty in temperature is less than 1 K. The CW-SR data were acquired in the limit where the time constant was independent of increasing pump time.

S-band (ca. 3.0 GHz) CW-SR data were acquired on a locally built spectrometer [44] equipped with a crossed-loop resonator (CLR) that is similar to a previously described resonator [45]. The CLR assembly, including the first-stage amplifier, was in a custom-built CryoIndustries (Atkinson, NH) cryostat with two thermocouples attached to the resonator for sample temperature measurement. Temperatures from 77 to 250 K were obtained by flowing gaseous N_2 through a coil submersed in liquid nitrogen. Temperatures below 77 K were obtained by liquid helium flow. A Conductus LTC 10 temperature controller was used for temperature regulation.

X-band pulsed ELDOR, inversion recovery, and ED-SR data were acquired on a locally built spectrometer equipped with a 1 kW pulsed TWT, a TE_{102} cavity resonator, and a quartz dewar insert [46,47]. The resonator was overcoupled to $Q \sim 120–150$. The samples were cooled by nitrogen gas flowing through a coil submersed in liquid nitrogen. A Wavetek MicroSweep Model 965 was the frequency source for the first pulse of the 3-pulse experiments. A pair of General Microwave PIN diode SP2T switches (F9120AH) was used to rapidly switch between the two frequency sources. For the pulsed ELDOR experiments the pump (v_2) and observe (v_1) frequencies were set symmetrically about the frequency of the resonator to generate similar B_1 for the pump and observe pulses. A 180° pulse was 64 ns long. The pulse sequence for inversion recovery and inversion ELDOR (IE) was 180°–τ–90°–T–180°–T–echo in which τ was varied and $T = 160$ ns was the time between the end of the second pulse and the beginning of the third pulse. The first 180° pulse was at v_1 or v_2, for the inversion recovery or inversion ELDOR experiments, respectively. The second and third pulses were at v_1. The pulse sequence for ED-SR and saturation ELDOR (SE) was (low-power 6 μs pulse)–τ–90°–T–180°–T–echo. The first pulse was at v_1 or v_2, for the ED-SR or saturation ELDOR experiments, respectively. For all ELDOR experiments the position of the pump pulse was on the center-line of the CW-absorption spectrum and the observe pulses were on the adjacent high-field line (Fig. 1). The inversion recovery and ED-SR data were obtained for the center line of the spectrum with all three pulses at the same frequency. Corrections for instrumental artifacts were performed by subtraction of data obtained with the Wavetek turned off. In the absence of an ELDOR effect a pulse at v_2 has no effect on echo intensity at v_1. An ELDOR enhancement or reduction is defined by the ratio of the echo intensity at v_1 following a pulse at v_2 relative to the echo intensity without a preceding pulse at v_2.

ELDOR data were not obtained at S-band because the resonator could not be overcoupled to low enough Q to permit ELDOR frequencies corresponding to two resolved hyperfine lines into the resonator. Also, the 20 W TWT that was available could not excite a large enough bandwidth for the ELDOR experiment.

2.3. Analysis of the pulsed EPR data

The CW-SR data were analyzed first by fitting to a single exponential using a Levenberg–Marquardt algorithm. For recovery curves that did not fit well to a single exponential, Provencher's Multifit routine [48] was used to fit the data to the sum of exponentials.

A 16-level model was used to analyze the contributions of relaxation processes to the ELDOR curves (Fig. 2). For each radical the relative intensities of the hyperfine lines were used to calculate the probabilities of nuclear spin flips between pairs of adjacent hyperfine lines. In the simulations four hyperfine lines were included in the calculation: the hyperfine lines that were pumped on and observed, plus the adjacent hyperfine lines to high- and low-field of those lines. The other hyperfine lines were considered to make negligible contributions to the overall relaxation. In the inversion recovery or saturation recovery experiments transition $3 \rightarrow 4$ is both excited and observed. In the ELDOR experiments transition $1 \rightarrow 2$ is excited by the first pulse and transition $3 \rightarrow 4$ is observed. Four relaxation times were used to model the return of the spin system to equilibrium. T_{1e} equilibrates levels that differ only in M_s. T_{1n} equilibrates levels that differ only in M_I. T_{x1} is
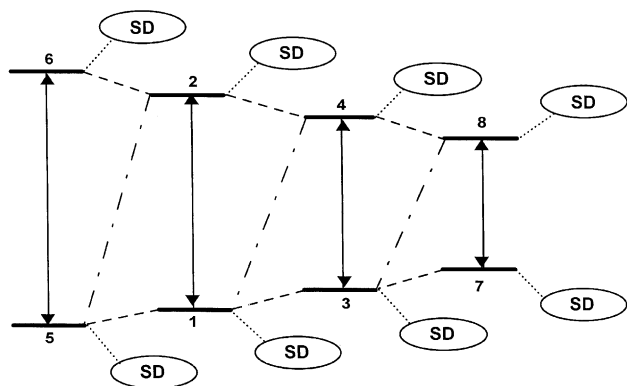
Fig. 2. Energy level model used to simulate the pulsed ELDOR curves. Each of the eight levels (1–8) is connected by spin diffusion to another levels, which produces a 16-level model. For the ELDOR experiments transition $1 \rightarrow 2$ was pumped and transition $3 \rightarrow 4$ was observed. For inversion recovery and ED-SR experiments, transition $3 \rightarrow 4$ was excited and observed. Time constants T_{1e} (—), T_{1n} (- - -), T_{x1} (- · - · -), and T_s (· · ·) were adjusted to obtain the best fits to the experimental data.

the cross-relaxation process with $\Delta M_s + \Delta M_I = 0$ ($\Delta M_s = \pm 1$, $\Delta M_I = \mp 1$). T_{x2} ($\Delta M_s + \Delta M_I = \pm 2$) was assumed to be significantly longer than T_{x1} [49] and was not included in the model. Eight additional levels are connected to levels 1–8 by spin diffusion with time constant T_s (Fig. 2).

Observation of an ELDOR enhancement indicates that the population of level 3 is high and/or the population of level 4 is low (Fig. 2), which arises when cross-relaxation occurs more rapidly than other relaxation processes. Thus the observation of an ELDOR enhancement indicates that $T_{x1} < T_{1e}, T_n$. The diagram in Fig. 2 is drawn assuming that $A_H > 0$. If $A_H < 0$ then T_{x1} would connect levels 2 and 3, but short T_{x1} would still result in an ELDOR enhancement.

Mathcad (MathSoft, Cambridge, MA) routines were written based on the model in Fig. 2. The model was applied only at temperatures where the rate of methyl rotation was fast relative to the hyperfine splitting. The time dependence of the population of each level was expressed in terms of the four time constants and the deviation of the instantaneous population from the equilibrium Boltzmann population [50,51]. The evolution of the populations was calculated using numerical integration with a fourth-order Runge–Kutta algorithm. For the inversion recovery and inversion ELDOR experiments the initial populations of the levels that are involved in the transition that was excited by the first pulse were adjusted to match the observed extent of inversion. Complete inversion was not attained, which may be due to very fast spectral diffusion that moves spins off resonance during the inverting pulse or to incomplete excitation of the inhomogeneously broadened lines. T_{1e}, T_{x1}, T_{1n}, and T_s were adjusted iteratively to simultaneously give the best fit to both the inversion recovery and inversion-ELDOR data. Curves initially

were modeled assuming negligible spin diffusion. If a single set of parameters did not fit both sets of data, spin diffusion was introduced. T_s and the populations of the spin bath levels were adjusted to account for the fastest component in the inversion recovery curve and for the magnitude of the ELDOR reduction or enhancement. For the ELDOR enhancements the initial rise is determined by T_{x1}. The subsequent decline is determined by T_{1e} and T_{1n}. A decrease below the equilibrium value of 1 indicates that $T_{1n} < T_{1e}$. At constant T_{1e} and T_{1n}, shorter T_{x1} gives larger ELDOR enhancements. The values of T_{x1} and T_{1e} are well defined by the ELDOR curves and uncertainties are estimated to be about 10%, although uncertainties in T_{1e} are larger when $T_{1e} \sim T_{1n}$. For these samples, uncertainties in T_{1n} are substantially larger than 10%, because nuclear spin relaxation makes a much smaller contribution to the ELDOR curves.

The values of T_{1e}, T_{x1}, and T_{1n} obtained by fitting the saturation ELDOR curves were consistent with values obtained by inversion ELDOR. However, the Mathcad routines that were used to analyze the inversion ELDOR curves were not successful in modeling the magnitude of the enhancements or reductions in the saturation ELDOR curves, which is attributed to an incomplete description of the events that occur during the long saturating pulses. During the long saturating pulse, magnetization can move to other lines in the spectrum, not just the four transitions that are included in the model. In addition, the saturation ELDOR results in a less well-defined initial state for the observed magnetization than for inversion ELDOR, which complicates quantitative modeling of the data. In the inversion ELDOR experiment, hard (non-selective) pulses were used for the pump and observe pulses, so the fraction of the "pumped" line that is excited is comparable to the fraction of the "observed" line that is detected, which results in a relatively well-defined initial state for the observed magnetization. In the saturation ELDOR experiments the initial long low-power saturating pulse is relatively selective. Although $B_1 = 0.2$–0.6 G, the $6\,\mu s$ length of the pulse means that $1/t_p \sim 0.06$ G, which excites a very small fraction of the "pumped" line. The shorter observing pulses had B_1 about 3 G, which excites a substantial fraction of the "observed" line.

2.4. Analysis of the temperature dependence of T_{1e}

The temperature dependence of $1/T_{1e}$ was fitted to

$$
\frac{1}{T_{1e}} = A_{dir} + A_{Ram} \left(\frac{T}{\theta_D} \right)^9 J_8 \left(\frac{\theta_D}{T} \right)
$$
$$
+ A_{loc} \left(\frac{e^{\Delta_{loc}/T}}{(e^{\Delta_{loc}/T} - 1)^2} \right) + A_{Me} \left[\frac{2\tau_c}{1 + \omega^2 \tau_c^2} \right]
$$
$$
+ A_{Me2} \left[\frac{2\tau_{c2}}{1 + \omega^2 \tau_{c2}^2} \right], \tag{1}
$$

Table 1
Contributions to spin–lattice relaxation determined by fitting to Eq. (1)[a]

Irradiated solid	Temperature range studied (K)	Raman: A_{Ram}, θ_D	Methyl rotation: E_a, τ_0 (s), ε^b, A_{Me} (X), A_{Me} (S)	Methyl rotation: E_a, τ_0 (s), ε^b, A_{Me2} (X), A_{Me2} (S)
Dimethyl-malonic acid	18–295	2.6×10^4, 150	170, 6×10^{-13}, 0.4, 4.5×10^{14}, 5.5×10^{13}	250, 6×10^{-13}, 0.6, 1.5×10^{14}, 8×10^{13}
α-Amino isobutyric acid[c]	16–295	2.6×10^4, 150[d]	160, 6×10^{-13}, 0.4, 1.3×10^{15}, 9×10^{14}	600, 1×10^{-13}, 0.8, 1.5×10^{15}, 7×10^{14}
L-Valine[c]	16–330	2.0×10^4, 150[d]	165, 4×10^{-13}, 0.6, 1.2×10^{14}, 9×10^{13}	900, 2.1×10^{-14}, 0.45, 1.5×10^{15}, 8×10^{14}

[a] Energies in Kelvin. To convert from Kelvin to kJ/mol multiply by 8.37×10^{-3}.
[b] Davidson–Cole distribution parameter [55].
[c] Contributions from a third thermally activated methyl or amino group rotation process are not included in the table but are discussed in the text.
[d] Contribution from the Raman process is significant only for a small temperature interval so there is substantial uncertainty in the parameters.

where T is the temperature in Kelvin, A_{dir} is the coefficient for the direct process, A_{Ram} is the coefficient for the Raman process, θ_D is the Debye temperature, and J_8 is the transport integral,

$$J_8\left(\frac{\theta_D}{T}\right) = \int_0^{\theta_D/T} x^8 \frac{e^x}{(e^x-1)^2}\, dx, \qquad (2)$$

A_{loc} is the coefficient for the contribution from a local vibrational mode, Δ_{loc} is the energy for the local mode in Kelvin, A_{Me} and A_{Me2} are the coefficients for the contributions from the thermally activated rotation of two inequivalent methyl groups, τ_c and τ_{c2} are the corresponding correlation times, which are equal to $\tau_0 e^{E_a/kT}$, E_a is the activation energy, and τ_0 is the pre-exponential factor. An Orbach process was not considered because there are no known low-lying electronic excited states for the radicals examined. Mathematical expressions for the temperature dependence of spin–lattice relaxation are taken from the following references: Raman process [52,53], local mode [20], and thermally activated process [54].

2.5. Strategy used in analyzing temperature dependence of T_{1e}

For each sample, the temperature dependence of $1/T_{1e}$ was fitted with the smallest number of contributing processes consistent with the experimental data. Comparison of T_{1e} at X-band and S-band allowed for the distinction between the effects of methyl rotation, which are frequency dependent, and contributions from other processes that are not frequency dependent. In temperature ranges where methyl rotation dominates T_{1e}, there are two adjustable parameters, τ_0 and E_a. The uncertainties in these parameters are decreased by requiring agreement with the data at both microwave frequencies. In temperature ranges where methyl-group rotation did not dominate spin–lattice relaxation, a Raman process and/or local vibrational mode dominated T_{1e}. The Raman process typically dominates at lower temperatures than local vibrational modes and results in a smaller slope in a plot of $\log(1/T_{1e})$ versus

$\log(T)$ than local vibrational modes [10]. Table 1 summarizes the parameters that were used to obtain the fit lines for the X-band and S-band data.

For these radicals, distributions of activation energies were used to model the contribution of methyl group rotation to T_{1e}. Radiation induced damage may contribute to the distribution in activation energies. Three distribution functions were examined. A Gaussian distribution or a Fang distribution [55] did not give as good fits to the temperature dependence of $1/T_{1e}$ as a Davidson–Cole distribution [55]. In the Fang distribution, interaction with the lattice leads to increased steric hindrance and there is a distribution of activation energies above a lower limit. In the Davidson–Cole distribution there is an upper limit on the activation energy and a distribution below that limit. This model has been widely used to interpret nuclear spin relaxation in solids [55].

3. Results

The time constants obtained as a function of temperature by (a) CW-SR using a pump time that was long relative to T_{1e}, (b) ED-SR with a saturating pulse of 6 μs, and (c) inversion recovery using an initial pulse of 64 ns were compared to determine the contribution of spectral diffusion. Although the recovery curves were not single exponentials, the temperature dependence of the time constants obtained by single exponential fits was compared to analyze qualitative trends. The recovery curves obtained by the three techniques for irradiated dimethyl-malonic acid at 77 K are shown in Fig. 3. The time constants for inversion recovery and ED-SR curves were significantly shorter than for the CW-SR curve. Similar trends in the recovery curves were observed for the radicals in irradiated α-amino isobutyric acid and in L-valine at all temperatures examined.

The widths of resolved hyperfine lines for these samples were 6–18 G. To determine if spin diffusion within a hyperfine line contributed to the electron spin relaxation, inversion recovery curves were measured as a
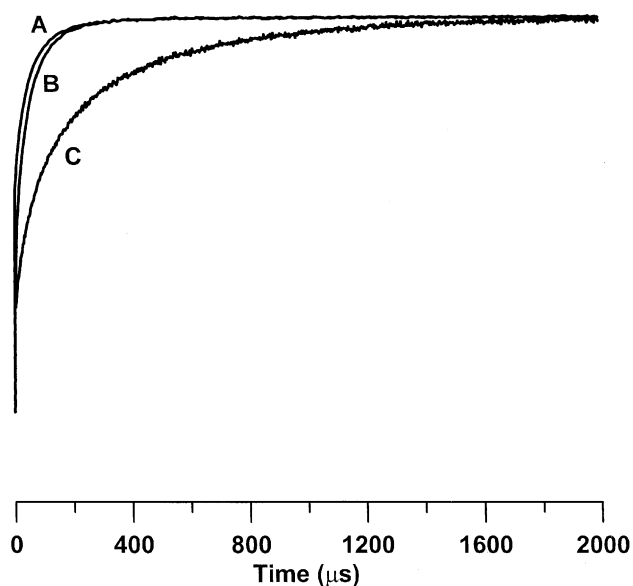
Fig. 3. Recovery curves at 77 K for the dimethyl-malonic acid radical, obtained by (A) inversion recovery with $B_1 = 1.5$ G, (B) ED-SR, and (C) CW-SR.

function of B_1 with $B_1 \sim 1.5$ G (90° pulse length $\sim$60 ns), $B_1 \sim 3.0$ G (90° pulse length $\sim$30 ns), and $B_1 \sim 6.0$ G (90° pulse length $\sim$15 ns). As B_1 is increased, a larger fraction of the hyperfine line is excited. If spin diffusion within the hyperfine line contributes to the recovery curve, the time constant will decrease as B_1 is increased. The results for each radical are discussed in the following paragraphs.

Pulsed ELDOR was used to determine the time constants for nuclear spin relaxation (T_{1n}) and cross-relaxation (T_{x1}) between resolved hyperfine lines and to separate these contributions from T_{1e}. By analysis of the various recovery curves, a consistent set of time constants was obtained for each sample. The temperature dependence of T_{1e} was modeled to determine the processes that dominate the spin–lattice relaxation. CW-SR data were obtained at two different microwave frequencies to test for thermally activated dynamic processes.

3.1. Dimethyl-malonic acid

The CW-absorption spectrum for the radical in γ-irradiated dimethyl-malonic acid is shown in Fig. 1A. The radical is formed by removal of a carboxyl group [56]. At room temperature the 7-line EPR spectrum is due to equivalent couplings to the protons of the two methyl groups. The line shape of the CW spectrum is approximately independent of temperature above 30 K, indicating that the rate of rotation of both methyl groups is fast relative to the hyperfine splitting. Hydrogen bonding dynamics for dimethyl-malonic acid have been studied by NMR [57]. In addition, CW-ELDOR studies of irradi-

ated dimethyl-malonic acid have shown that spectral diffusion processes, T_{x1} and T_{1n}, contribute to electron spin relaxation for this sample [56].

3.1.1. Spectral diffusion

The time constants obtained by single exponential fits to the recovery curves increased in the order: inversion recovery (at three different values of B_1) < ED-SR < CW-SR, which correlates with the length of the excitation pulse (Fig. 4). The dependence of the time constants on the length of the excitation pulse, and the observation that the inversion recovery and ED-SR curves did not fit well to single exponentials, indicate that spectral diffusion processes make substantial contributions to the inversion recovery and ED-SR curves, especially at low temperatures (Figs. 3 and 4).

The full width of a hyperfine line at half maximum is about 10 G (Fig. 1A). The time constants obtained by inversion recovery increased as B_1 was increased (Fig. 4), which indicates that spins excited by the pulse are exchanging energy with spins that were not excited by the pulse. Although $B_1 \sim 6.0$ G excited a significant portion of the hyperfine line, and thus is expected to suppress most of the spin diffusion, the time constants
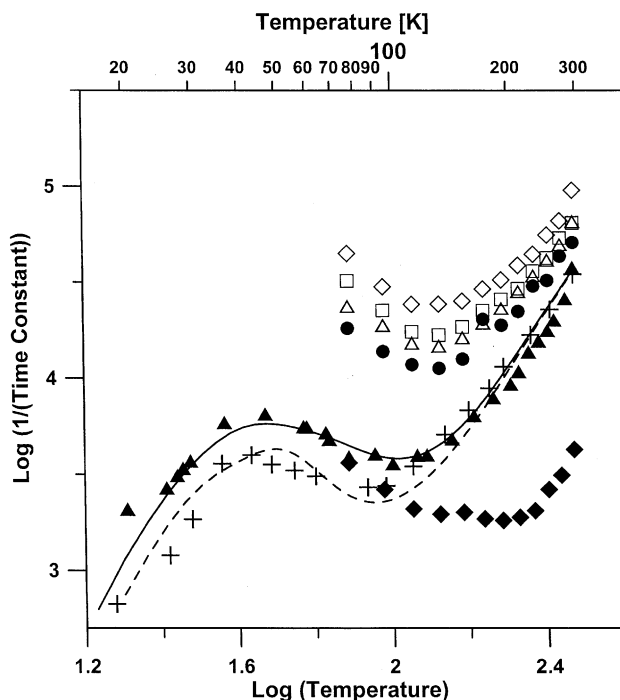

Fig. 4. Temperature dependence of the recovery rate constants for the dimethyl-malonic acid radical obtained from (◇) X-band inversion recovery with $B_1 = 1.5$ G, (□) X-band inversion recovery with $B_1 = 3.0$ G, (△) X-band inversion recovery with $B_1 = 6.0$ G, (●) X-band ED-SR, (▲) X-band CW-SR, (+) S-band CW-SR curves, and (◆) T_{1n} from simulations of the inversion recovery and inversion ELDOR curves. The parameters used to fit the temperature dependence of the (—) X-band and (---) S-band values of T_{1e} are summarized in Table 1.

obtained by ED-SR and CW-SR were longer than obtained by inversion recovery, which indicates that additional spectral diffusion processes contribute to the inversion recovery curves.

Pulsed ELDOR was used to characterize the additional spectral diffusion processes. Fig. 5 shows the temperature dependence of the inversion ELDOR curves that were obtained by pumping on the center-line (3250 G) and observing at the adjacent higher-field line (3272 G) (Fig. 1). ELDOR enhancements were observed at all temperatures examined between 77 and 295 K. The enhancements were attributed to rapid cross-relaxation, $T_{x1} < T_{1n}$, T_{1e}. The fits to selected inversion ELDOR data are shown in Fig. 5. T_{x1} (Fig. 6) increases from 12 μs at 77 K (19% enhancement) to 70 μs at 295 K (2% enhancement) (Fig. 5). Saturation ELDOR curves also showed enhancements, but the enhancement immediately following the 6 μs pulse was greater than for inversion ELDOR, due to cross-relaxation during the time of the pulse. The CW-SR data were obtained with pump times that were longer than T_{x1} and T_s and fitted reasonably well to single exponentials. T_{1e} values obtained by simulation of the ELDOR curves were in good agreement with the single exponential fits to the CW-SR curves. Therefore single exponential fits to the CW-SR curves are assumed to give reasonable estimates of T_{1e} even below 77 K, where ELDOR data were not obtained. Values of T_{1n} obtained from the simulations are

Fig. 6. Temperature dependence of T_{x1} for the radicals in γ-irradiated (●) dimethyl-malonic acid, (◆) α-amino isobutyric acid, and (▲) L-valine.

shown in Fig. 4. T_{1n} is 235 μs at room temperature, is about 500 μs between 233 and 113 K, and becomes comparable to T_{1e} below 113 K. The spin diffusion time constant, T_s, was about 10 μs from 77 to 295 K.

3.1.2. Temperature dependence of T_{1e}

At S-band and X-band, from about 15 to 130 K (Fig. 4), T_{1e} is dominated by a thermally activated process that is attributed to rotation of the methyl groups in the radical at a rate that is approximately equal to the microwave frequency (3 or 9.1 GHz). To fit the large temperature range over which $1/T_{1e}$ at X-band and S-band was enhanced, two activation energies ($E_a = 170$ K (1.4 kJ/mol) and 250 K (2.1 kJ/mol)) were used. Above 130 K the S-band and X-band values of T_{1e} were the same (Fig. 4), within experimental error, which indicated that the dominant relaxation process was not frequency dependent and thus not a thermally activated process. Above 130 K the temperature dependence of $1/T_{1e}$ is characteristic of the Raman process and the fit line was obtained with a Debye temperature of 150 K. Above about 230 K $1/T_{1e}$ increases more rapidly with increasing temperature than predicted by the Raman process, which is attributed to a contribution from a local mode. However, the contribution from this process is small enough that a range of values of Δ_{loc} between 1000 and 2500 K (~700–1750 cm^{-1}, ~8.4–21 kJ/mol), with correlated changes in A_{loc}, gave comparable fits to the experimental data. A mode in this energy range could be due to an internal vibration of the radical. Table 1 shows the parameters that were used to fit the $1/T_{1e}$ data at S-band and X-band.
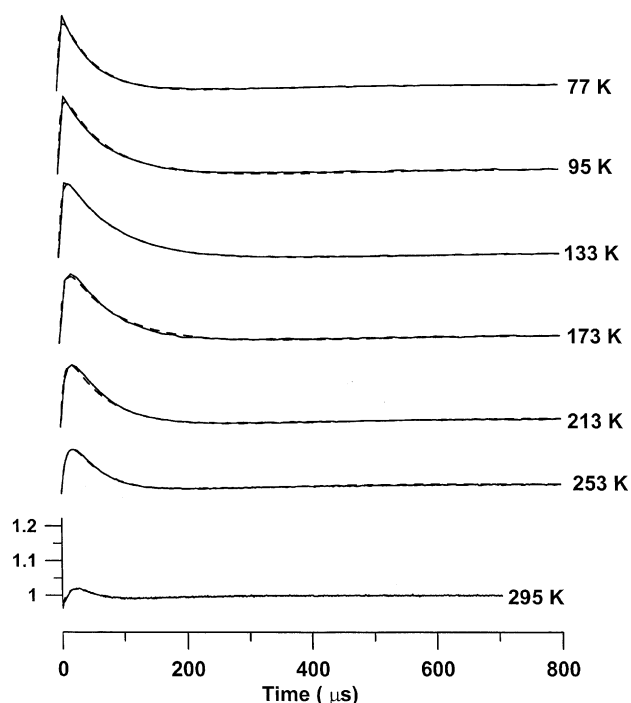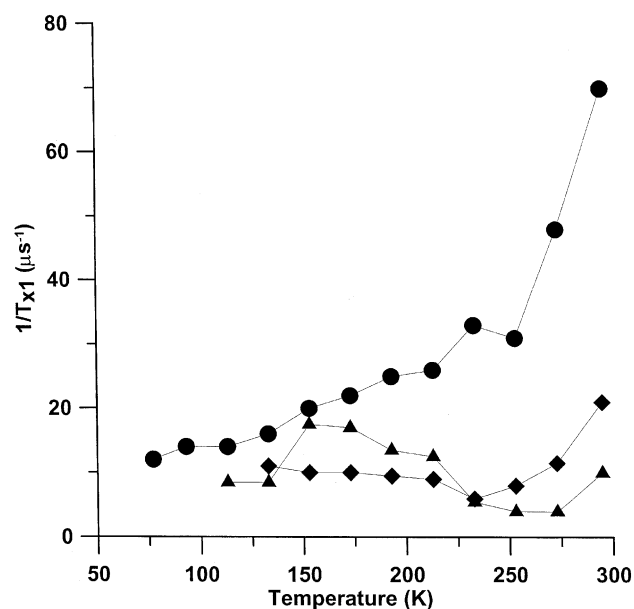

Fig. 5. X-band inversion ELDOR curves for the dimethyl-malonic acid radical at selected temperatures. The y-axis scale is the same for all traces, but is shown only for one trace. The enhancement increased from 2% at 295 K to 21% at 95 K. Simulations (–––) were calculated based on the model in Fig. 2.

3.2. α-Amino isobutyric acid

The major free radical in γ-irradiated α-amino isobutyric acid is formed by loss of an $-NH_3$ group [58–60]. The 7-line CW-EPR spectrum at room temperature is due to equivalent couplings to six methyl protons ($A_H \sim 22$ G). Although the radical in irradiated α-amino isobutyric acid is the same as in irradiated dimethyl-malonic acid, the full width at half height for each hyperfine line in α-amino isobutyric acid (~6 G, Fig. 1B) is narrower than in dimethyl-malonic acid (~10 G, Fig. 1A), which reflects the effects of each lattice on the radical. Below 113 K the spectrum changes reversibly because the rotation rate of one of the methyl groups is no longer fast relative to inequivalences in the electron–proton hyperfine couplings. Irradiated α-amino isobutyric acid has been studied by CW-EPR [58–60] and ENDOR [61,62] to determine the conformations of the radical at different temperatures. CW ELDOR showed enhancements below 283 K [56].

3.2.1. Spectral diffusion

The time constants obtained by single exponential fits to the recovery curves increased in the order: inversion recovery < ED-SR < CW-SR (Fig. 7), which suggests that spectral diffusion makes significant contributions to
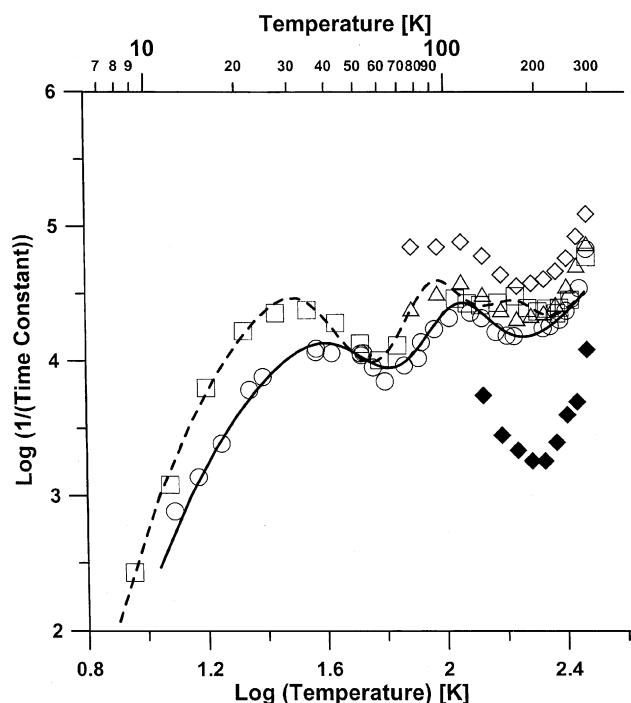
the recovery curves. Time constants obtained from inversion recovery curves increased in the order $B_1 = 1.5$ G < $B_1 = 3.0$ G < $B_1 = 6.0$ G. At 295 K the time constant obtained with $B_1 = 6.0$ was 1.2 times that obtained with $B_1 = 1.5$ G. This ratio increased to 1.4 at 77 K, which indicates that spin diffusion contributes more to the relaxation at lower temperatures. The shorter time constants obtained by inversion recovery with $B_1 = 6.0$ G than by CW-SR indicate that additional spectral diffusion processes contribute to the inversion recovery, even when B_1 is large enough to excite most of the linewidth.

Between 153 and 295 K the ELDOR curves (Fig. 8) were fitted using the MathCad model (Fig. 2). T_{x1} decreases from 21 μs (2% enhancement) at 295 K to 6 μs (17.5% enhancement) at 233 K then increases to 11 μs (10% enhancement) at 133 K (Figs. 6 and 8). The values of T_{1e} that were obtained by simulation of the ELDOR curves were in good agreement with the single exponential fits to the CW-SR curves. These values are therefore assumed to be reasonable estimates of T_{1e} even below 77 K, where ELDOR data were not obtained. Between 77 and 295 K $1/T_{1n}$ (Fig. 7) follows the trend in $1/T_{1e}$, suggesting that electron spin relaxation may enhance nuclear spin relaxation in this temperature range.

3.2.2. Temperature dependence of T_{1e}

The two maxima in the temperature dependence of $1/T_{1e}$ (Fig. 7) suggest that there are at least two dynamic processes with distinctly different activation energies. The fit line in Fig. 7 was obtained with $E_a = 160$ K (1.3 kJ/mol, which dominates between 10 and 65 K),
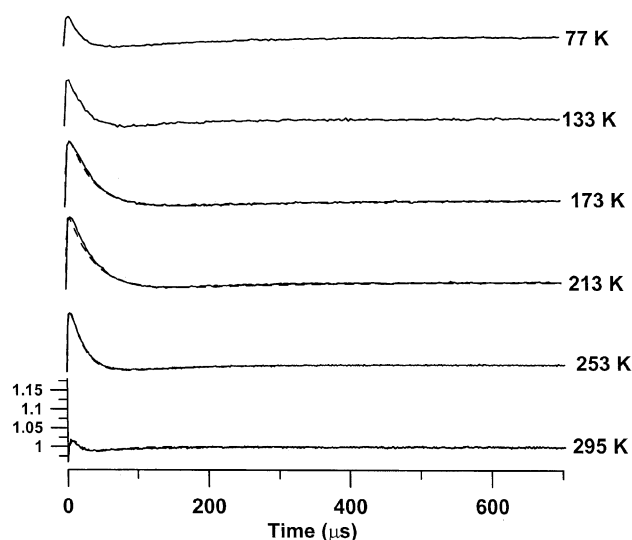
Fig. 7. Temperature dependence of the recovery rate constants for γ-irradiated α-amino isobutyric acid obtained by (◇) X-band inversion recovery with $B_1 = 3.0$ G, (△) X-band ED-SR, (□) S-band CW-SR, (○) X-band CW-SR, and (◆) T_{1n}. The parameters used to fit the temperature dependence of the (—) X-band and (---) S-band values of T_{1e} are summarized in Table 1.

Fig. 8. X-band inversion ELDOR curves for γ-irradiated α-amino isobutyric acid at selected temperatures. The y-axis scale is the same for all traces, but is shown only for one trace. The enhancement ranged from 2% at 295 K to 18% at 213 K and 5% at 77 K. Simulations (---) were calculated based on the model in Fig. 2.

$E_a = 600 \, \text{K}$ (5.0 kJ/mol, which dominates between 65 and 200 K), and a third process with $E_a = 1300 \, \text{K}$ (11 kJ/mol, which dominates between 200 and 253 K). Based on the temperature-dependent changes in the CW spectrum and prior reports of the inequivalence of rotational barriers for the methyl groups [63] the two processes with lower activation energies are attributed to methyl group rotation and the third process may be due to rotation of a lattice amino or methyl group. Above 253 K the Raman process dominated the relaxation, with a small contribution from a local vibrational mode. The parameters for these processes were not well defined, so the values used to fit the $1/T_{1e}$ data for irradiated dimethyl-malonic acid in this temperature interval were used. It is reasonable to assume that the local mode contribution would be similar for the same radical in the two hosts. There is substantial uncertainty in the parameters for the Raman process because of overlap with other contributions.

3.3. L-Valine

The radical observed by EPR following γ-irradiation of L-valine depends upon the temperature for irradiation and observation [64–66]. EPR studies have been performed for radicals formed by loss of a proton or an amino group [64–66]. For the sample studied here, which was irradiated at room temperature, the number of hyperfine lines and the ratios of the intensities of the lines (Fig. 1C) indicate that the major radical exhibits approximately equivalent couplings ($A_H \sim 20 \, \text{G}$) to 8 hydrogens (6 methyl hydrogens and 2 hydrogens from the –CH$_2$ group bonded to the radical carbon). In addition, partially resolved amino nitrogen couplings are observed in the CW-spectrum. The structure drawn in Fig. 1C is based on these observations. Below 150 K dramatic changes in the CW line shape are observed, which are attributed to rotation of one of the methyl groups at a rate approximately equal to the inequivalence in the hyperfine splittings.

3.3.1. Spectral diffusion

Single exponential fits to the inversion recovery curves gave time constants that are shorter than those obtained by either ED-SR or CW-SR (Fig. 9), which are approximately equal, within experimental error, between 77 and 213 K. Thus, for this sample, the 6 μs pulse used in ED-SR and the long pulse (hundreds of μs) used in CW-SR set up approximately the same initial conditions for relaxation. Inversion recovery curves were obtained using $B_1 = 1.5$, 3.0, and 6.0 G. These values of B_1 all are small relative to the 18-G full width of a hyperfine line at half height. Throughout the temperature range examined (77–295 K) the time constants obtained using $B_1 = 1.5 \, \text{G}$ were 40–50% shorter than the time constants obtained using $B_1 = 6.0 \, \text{G}$, indicating sub-
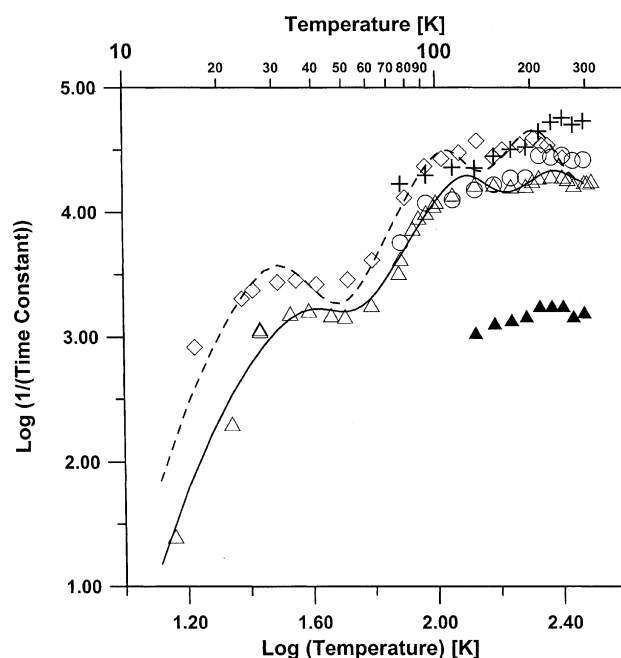

Fig. 9. Temperature dependence of the recovery rate constants for γ-irradiated L-valine obtained by (+) X-band inversion recovery with $B_1 = 3.0 \, \text{G}$, (○) X-band ED-SR, (◇) S-band CW-SR, (△) X-band CW-SR, and (▲) T_{1n}. The parameters used to fit the temperature dependence of the (—) X-band and (---) S-band values of T_{1e} are summarized in Table 1.

stantial contributions from spin diffusion. The time constants obtained by inversion recovery using $B_1 = 6.0 \, \text{G}$ were shorter than those obtained by either ED-SR or CW-SR, indicating that additional spectral diffusion processes contribute to the inversion recovery curves.

Pulsed ELDOR curves were obtained by pumping on the center line (3250 G) and observing the adjacent high-field line (3270 G) (Fig. 1). ELDOR enhancements were observed from 77 to 295 K (Fig. 10). The values obtained for T_{x1} (Fig. 6) ranged from 4 to 17 μs between 77 and 295 K. Between 113 and 295 K the inversion ELDOR recovery after the initial enhancement did not go below equilibrium, which indicated that the nuclear relaxation time, T_{1n}, was much longer than T_{1e} and T_{x1}. The values for T_{1n} ranged from 580 to 950 μs (Fig. 9). Below 77 K the CW-SR curves fit well to a single exponential and the time constants were assigned as T_{1e}. At higher temperatures, the CW-SR curves did not fit well to a single exponential, but the time constants obtained by a single exponential fit were consistent with the values of T_{1e} that were used to fit the ELDOR curves.

3.3.2. Temperature dependence of $1/T_{1e}$

The temperature dependence of $1/T_{1e}$ obtained at X-band and S-Band (Fig. 9) shows three temperature ranges in which thermally activated processes dominate relaxation. Between about 12 and 42 K T_{1e} is dominated
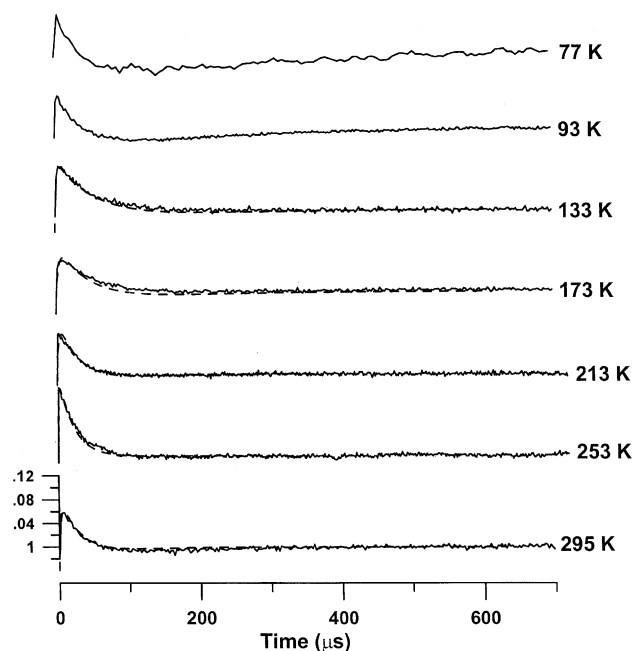
Fig. 10. X-band inversion ELDOR curves for γ-irradiated L-valine at selected temperatures. The y-axis scale is the same for all traces, but is shown only for one trace. The enhancement ranged from 6% at 295 K to 12% at 253 K. Simulations (– – –) were calculated based on the model in Fig. 2.

by methyl rotation with $E_a = 165\,K$ (1.4 kJ/mol). Between 42 and 200 K T_{1e} is dominated by rotation of a second methyl group with $E_a = 900\,K$ (7.5 kJ/mol). Between 200 and 253 K the small effect of a third thermally activated process is observed, which is attributed to rotation of the $-NH_3$ group with $E_a = 1900\,K$ (16 kJ/mol).

4. Discussion

4.1. Effects of cross-relaxation

For the radicals in irradiated dimethyl-malonic acid, α-amino isobutyric acid, and L-valine, time constants obtained by inversion recovery, ED-SR, and CW-SR were different, which is attributed to varying contributions from spectral diffusion processes. Pulsed ELDOR enhancements were observed between 77 and 295 K, which is attributed to rapid cross-relaxation ($T_{x1} < T_{1e}$, T_{1n}). The observed ELDOR enhancements for irradiated dimethyl-malonic acid and α-amino isobutyric acid are in good agreement with CW-ELDOR enhancements observed by Kispert et al. [56] between 150 and 260 K. The CW-ELDOR enhancements were attributed to rapid cross-relaxation due to rotation of a methyl group at a rate comparable to the microwave frequency. For the three radicals examined in this study, fast cross-relaxation was observed over large temperature ranges (77–

295 K), which suggests that multiple methyl groups in the radical and in the lattice, with different activation energies, contribute to the cross-relaxation and resulting ELDOR enhancements.

In the temperature range in which rapid cross-relaxation was observed, the CW-SR curves for the three samples did not fit well to a single exponential, which could be due to orientation dependence of relaxation times, multiple contributing processes, and/or multiple radicals in the sample. The CW spectra show no evidence of multiple radicals and the substantial elapsed time between irradiation and EPR experiments implies that only the most persistent radicals will be observed. The observation of single exponential fits in some temperature intervals also argues against contributions from multiple radicals. In the absence of single crystal studies, it is difficult to assess the importance of orientation dependence.

When the CW-SR curves were fit to a sum of two exponentials, the time constant for the short component was longer than T_{x1} and neither time constant was consistent with the value of T_{1e} required to fit the EL-DOR curves. When the CW-SR curves were fit to the sum of three exponentials, the intermediate time constant had the largest weighting, was similar to the single-component fit, and was consistent with the value of T_{1e} required to fit the ELDOR data. The longer time constant was similar to T_{1n}, but the shorter time constant did not match with T_{x1}, and there was substantial scatter in the values. Thus it appears that the long pulses used to obtain the CW-SR curves did not fully eliminate contributions from spectral diffusion processes. Cross relaxation during the long pulse may create energy level populations for which the subsequent return to equilibrium is dominated by T_{1e}, but with additional contributions from spectral diffusion processes. We conclude that when cross-relaxation is fast, long-pulse CW-SR curves are not immune from the effects of spectral diffusion.

The effects of cross-relaxation during the time of the pulse also can be detected by comparison of inversion ELDOR and saturation ELDOR curves. In the saturation ELDOR curves (not shown) the enhancement immediately following the pulse is greater than in inversion ELDOR.

4.2. Temperature dependence of T_{1e}

Even though the same radical is present in the irradiated dimethyl-malonic acid and α-amino isobutyric acid, the temperature dependence of $1/T_{1e}$ is distinctly different for the two host lattices. In irradiated dimethyl-malonic acid, the barriers to rotation of the two methyl groups of the radical are about the same, while in irradiated α-amino isobutyric acid the barriers to rotation for the two methyl groups are distinctly different. These

findings for irradiated α-amino isobutyric acid agree with the CW results obtained by Box and Freund [60]. The activation energies for rotation of the methyl group that dominates T_{1e} between 10 and 65 K are approximately the same for dimethyl-malonic acid (170 K, 1.4 kJ/mol) and α-amino isobutyric acid (160 K, 1.3 kJ/mol), indicating that the barrier to rotation may have larger contributions from steric effects within the radical, rather than contributions imposed by the lattice. The barrier to rotation of the second methyl group is much higher in α-amino isobutyric acid (600 K, 5.0 kJ/mol) than in di-methyl-malonic acid (250 K, 2.1 kJ/mol), which indicates that steric interaction with the lattice has a larger impact for this methyl group than for the other methyl group.

The radical in irradiated L-valine has two distinctly different barriers to methyl group rotation: $E_a = 165$ (1.4 kJ/mol) and 900 K (7.5 kJ/mol). NMR studies between 130 and 500 K showed the effects on the temperature dependence of $1/T_{1n}$ due to one methyl group with $E_a = 1360$ K (11.3 kJ/mol) [12,16]. Rotation of the methyl group in the radical with the lower energy barrier may be too fast to detect in the NMR studies. For the second methyl group the higher barrier to rotation observed by NMR (1360 K, 11.3 kJ/mol) than by EPR (900 K, 7.5 kJ/mol) may indicate that γ-irradiation of L-valine caused the radical that is formed to reorient in the lattice and change the barrier. Also, the radical is a defect in the lattice, which may change the local motional barriers. Small effects of amino group rotation are observed in the X-band and S-band CW-SR data. The activation energy for rotation of the amino groups in the radical ($E_a = 1900$ K, 15.8 kJ/mol) is much lower than for the non-irradiated solid ($E_a = 4500$ K, 37.4 kJ/mol), which may be due to the difference in the hydrogen bonding involving the radical with the non-irradiated valine.

In the temperature ranges where methyl rotation did not affect T_{1e} (above 120 K for the radical in dimethyl-malonic acid, above 250 K for the radical in α-amino isobutyric acid, and above 270 K for the radical in L-valine), the $1/T_{1e}$ data could be fitted using a Raman process and local vibrational modes. The same parameters could be used to fit the Raman process and local vibrational modes for the radical in α-amino isobutyric acid and dimethyl-malonic acid (Table 1).

5. Conclusion

For the three samples examined, cross-relaxation induced by rotation of methyl groups at rates comparable to the electron Larmor frequency makes large contributions to inversion recovery and ED-SR curves. Using long-pulse CW-SR the effects of fast cross-relaxation could be suppressed, but the recovery curves still included contributions from spectral diffusion. The time constant obtained by fitting the CW-SR curves to a single exponential or the intermediate value of a three-component fit are consistent with the values of T_{1e} required to model the ELDOR curves. The large effects of dynamic processes on electron spin relaxation could be distinguished from relaxation processes that are not frequency dependent by comparing values of T_{1e} obtained at S-band and X-band. Activation energies for methyl and amino group rotation between 160 (1.3 kJ/mol) and 1900 K (16 kJ/mol) were obtained by analysis of the temperature dependence of $1/T_{1e}$ in temperature intervals where the dynamic process dominates T_{1e}.

References

[1] S.S. Eaton, G.R. Eaton, Biol. Magn. Reson. 19 (2000) 29–154.
[2] K.J. Standley, R.A. Vaughn, Electron Spin Relaxation Phenomena in Solids, Plenum Press, New York, 1969.
[3] A. Abragam, B. Bleaney, Electron Paramagnetic Resonance of Transition Ions, Oxford University Press, London, 1970.
[4] I. Bertini, G. Martini, C. Luchinat, in: C.P. Poole Jr., H. Farach (Eds.), Handbook of Electron Spin Resonance, American Institute of Physics, NY, 1994, pp. 51–77.
[5] C.P. Scholes, R.A. Isaacson, G. Feyer, Biochim. Biophys. Acta 244 (1971) 206–210.
[6] M.B. Yim, L.C. Kuo, M.W. Makinen, J. Magn. Reson. 46 (1982) 247–256.
[7] M.W. Makinen, M.B. Yim, Proc. Natl. Acad. Sci. USA 78 (1981) 6221–6225.
[8] M.W. Makinen, G.B. Wells, Metal Ions Biol. Syst. 22 (1987) 129–206.
[9] J.W. Orton, Electron Paramagnetic Resonance, Gordon and Breach, New York, 1968.
[10] Y. Zhou, B.E. Bowler, G.R. Eaton, S.S. Eaton, J. Magn. Reson. 139 (1999) 165–174.
[11] S. Idziak, N. Pislewski, Chem. Phys. 111 (1987) 439–443.
[12] E.R. Andrew, W.S. Hinshaw, M.G. Hutchins, R.O.I. Sjöblom, P.C. Canepa, Mol. Phys. 32 (1976) 795–806.
[13] P.A. Beckmann, F.A. Fusco, A.E. O'Neill, J. Magn. Reson. 59 (1984) 63–70.
[14] P.A. Beckmann, H.A. Al-Hallaq, A.M. Fry, A.L. Plofker, B.A. Roe, J. Chem. Phys. 100 (1994) 752–753.
[15] P.A. Beckmann, A.I. Hill, E.B. Kohler, H. Yu, Phys. Rev. B 38 (1988) 11098–11111.
[16] E.R. Andrew, W.S. Hinshaw, M.G. Hutchins, J. Magn. Reson. 15 (1974) 196–200.
[17] M. Brustolon, T. Cassol, L. Micheletti, U. Segre, Mol. Phys. 57 (1986) 1005–1014.
[18] S. Clough, F. Poldy, J. Chem. Phys. 51 (1969) 2076–2084.

[19] D.W. Feldman, J.G. Castle Jr., G.R. Wagner, Phys. Rev. 145 (1966) 237–240.

[20] J.G. Castle Jr., D.W. Feldman, Phys. Rev. A 137 (1965) 671–673.

[21] J.G. Castle Jr., D.W. Feldman, J. Appl. Phys. 36 (1965) 124–128.

[22] V.I. Muromtsev, N.Ya. Shteinshneider, S.N. Safranov, V.P. Golikov, A.I. Kuznetsov, G.M. Zhidomirov, Fiz. Tverd. Tela 17 (1975) 813–814 (pp. 517–519 in transl.).

[23] D. Kivelson, J. Chem. Phys. 33 (1960) 1094–1106.

[24] R. Wilson, D. Kivelson, J. Chem. Phys. 44 (1966) 154–168.

[25] J.-L. Du, G.R. Eaton, S.S. Eaton, J. Magn. Reson. A 119 (1996) 240–246.

[26] B.T. Ghim, J.-L. Du, S. Pfenninger, G.A. Rinard, R.W. Quine, S.S. Eaton, G.R. Eaton, Appl. Radiat. Isot. 47 (1996) 1235–1239.

[27] B. Rakvin, N. Maltar-Strmecki, P. Cevc, D. Arcon, J. Magn. Reson. 152 (2001) 149–155.

[28] M. Brustolon, A.L. Maniero, M. Bonoro, U. Segre, Appl. Magn. Reson. 11 (1996) 99–113.

[29] K.M. Salikov, Yu.D. Tsvetkov, in: L. Kevan, R.N. Schwartz (Eds.), Time Domain Electron Spin Resonance, Wiley, New York, 1979, pp. 231–277.

[30] M.K. Bowman, L. Kevan, in: L. Kevan, R.N. Schwartz (Eds.), Time Domain Electron Spin Resonance, Wiley, New York, 1979, pp. 68–105.

[31] P.W. Anderson, Phys. Rev. 109 (1958) 1492–1505.

[32] E.L. Wolf, Phys Rev. 142 (1966) 555–569.

[33] D. Tse, S.R. Hartmann, Phys. Rev. Lett. 21 (1968) 511–514.

[34] S.S. Eaton, G.R. Eaton, J. Magn. Reson. A 102 (1993) 354–356.

[35] N. Blombergen, Physica 15 (1949) 386–426.

[36] W.Th. Wenckebach, N.J. Poulis, in: V. Hovi (Ed.), 17th Congess Ampere, North-Holland, Amsterdam, 1973, pp. 120–142.

[37] M.K. Bowman, L. Kevan, Disc. Faraday Soc. 63 (1977) 7–17.

[38] M.K. Bowman, J.R. Norris, J. Phys. Chem. 86 (1982) 3385–3390.

[39] L. Kevan, P.A. Narayana, in: M.N. Dorio, J.H. Freed (Eds.), Multiple Electron Resonance Spectroscopy, Plenum Press, New York, 1979, pp. 288–298.

[40] A.A. Manenkov, Yu.E. Pol'skii, Sov. Phys. JETP 45 (1963) 1425–1429 (18 (1964) 985–987 in transl.).

[41] A.A. Manenkov, A.M. Prokhorov, Sov. Phys. JETP 42 (1962) 75–83 (pp. 54–59 in transl.).

[42] A.A. Manenkov, V.A. Milyaev, A.M. Prokhorov, Sov. Phys. Solid State 4 (1962) 388–391 (pp. 280–283 in transl.).

[43] R.W. Quine, S.S. Eaton, G.R. Eaton, Rev. Sci. Instrum. 63 (1992) 4252–4262.

[44] G.A. Rinard, R.W. Quine, R. Song, G.R. Eaton, S.S. Eaton, J. Magn. Reson. 140 (1999) 69–83.

[45] G.A. Rinard, R.W. Quine, B.T. Ghim, S.S. Eaton, G.R. Eaton, J. Magn. Reson. 122 (1996) 50–57.

[46] R.W. Quine, G.R. Eaton, S.S. Eaton, Rev. Sci. Instrum. 57 (1987) 1709–1724.

[47] G.A. Rinard, R.W. Quine, J.R. Harbridge, R. Song, G.R. Eaton, S.S. Eaton, J. Magn. Reson. 140 (1999) 218–227.

[48] S.W. Provencher, J. Chem. Phys. 64 (1976) 2772–2777.

[49] R. Angelone, C. Forte, C. Pinzino, J. Magn. Reson. 101 (1993) 16–22.

[50] J.S. Hyde, J.C.W. Chien, J.H. Freed, J. Chem. Phys. 48 (1968) 4211–4226.

[51] M. Nechtschein, J.S. Hyde, Phys. Rev. Lett. 24 (1970) 672–674.

[52] A. Abragam, The Principles of Nuclear Magnetism, Oxford University Press, London, 1961, pp. 405–409.

[53] J. Murphy, Phys. Rev. 145 (1966) 241–247.

[54] V.A. Atsarkin, V.V. Demidov, G.A. Vasneva, Phys. Rev. B 56 (1997) 9448–9453.

[55] P.A. Beckmann, Phys. Rep. 171 (1988) 85–128.

[56] L.D. Kispert, K. Chang, C.M. Bogan, J. Chem. Phys. 58 (1973) 2164–2176.

[57] W. Scheubel, H. Zimmermann, U. Haeberlen, J. Magn. Reson. 80 (1988) 401–416.

[58] P. Neta, W. Fessenden, J. Phys. Chem. 74 (1970) 2263–2266.

[59] M. Fujimoto, W.A. Seddon, D.R. Smith, J. Chem. Phys. 48 (1968) 3345–3350.

[60] H.C. Box, H.G. Freund, J. Chem. Phys. 44 (1966) 2345–2348.

[61] M. Iwasaki, H. Muto, J. Chem. Phys. 61 (1975) 5315–5320.

[62] O. Burghaus, A. Toth-Kischkat, R. Klette, K. Möbius, J. Magn. Reson. 80 (1988) 383–388.

[63] J.W. Wells, H.C. Box, J. Chem. Phys. 46 (1967) 2935–2938.

[64] W. Gordy, H. Shields, Bull. Am. Phys. Soc. 1 (1956) 267.

[65] S.Z. Shulga, A.I. Telyatnik, Ukr. Fiz. Zh. 9 (1964) 185–191.

[66] H.C. Box, H.G. Freund, E.E. Budzinski, J. Chem. Phys. 46 (1967) 4470–4473.